

# Terpyridine–Triarylborane Conjugates for the Dual Complexation of Zinc(II) Cation and Fluoride Anion

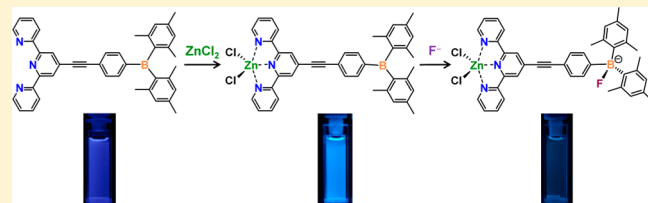
Young Hoon Lee,<sup>†</sup> Nguyen Van Nghia,<sup>†</sup> Min Jeong Go,<sup>‡</sup> Junseong Lee,<sup>‡</sup> Sang Uck Lee,<sup>\*,†</sup> and Min Hyung Lee<sup>\*,†</sup>

<sup>†</sup>Department of Chemistry and EHSRC, University of Ulsan, Ulsan 680-749, Republic of Korea

<sup>‡</sup>Department of Chemistry, Chonnam National University, Gwangju 500-757, Republic of Korea

## Supporting Information

**ABSTRACT:** A series of ditopic terpyridine–triarylborane conjugates (**1–3**) in which 4′-ethynylterpyridine is linked to the para, meta, and ortho positions of the phenyl ring of dimesitylphenylborane (Mes<sub>2</sub>PhB), respectively, were prepared to investigate the dual complexation behavior of the conjugates toward Zn(II) cation and fluoride anion. The crystal structures of the corresponding Zn(II) complexes (L·ZnCl<sub>2</sub>, L = **1–3**) reveal the formation of a 1:1 adduct between ZnCl<sub>2</sub> and a conjugate, with a five-coordinate Zn(II) center bound to three nitrogen atoms and two chlorine atoms. In particular, the structure of ortho-substituted **3**·ZnCl<sub>2</sub> in comparison with that of **3** indicates the presence of  $\pi$ – $\pi$  interactions between the mesityl ring and ethynylene–pyridine fragment in **3**·ZnCl<sub>2</sub>. UV/vis absorption and fluorescence spectra of **1–3** display low-energy bands mainly assignable to a  $\pi(\text{Ar}) \rightarrow \pi_p(\text{B})$  (Ar = Mes and/or phenylene–ethynylene) charge transfer (CT) transition. The transition in Zn(II) complexes has a  $\pi(\text{Mes}) \rightarrow \pi^*(\text{Ar})$  (Ar = terpyridine–ethynylene) intramolecular CT nature with red shifts of both the absorption and emission bands in comparison to those of free conjugates. These spectroscopic features are further supported by TD-DFT calculations. UV/vis absorption and fluorescence titration experiments of **1–3** toward Zn(II) and fluoride ion, respectively, show that while the absorption and fluorescence bands underwent gradual quenching upon addition of fluoride, the addition of ZnCl<sub>2</sub> gave rise to the red shifts of both bands. Fluoride titration experiments of Zn(II) complexes also resulted in gradual quenching of both the absorption and emission bands accompanied by the disappearance of emission color. Sequential addition of ZnCl<sub>2</sub> and fluoride to the conjugates reproduced the above binding behavior with an emission color change from deep blue to sky blue to dark.



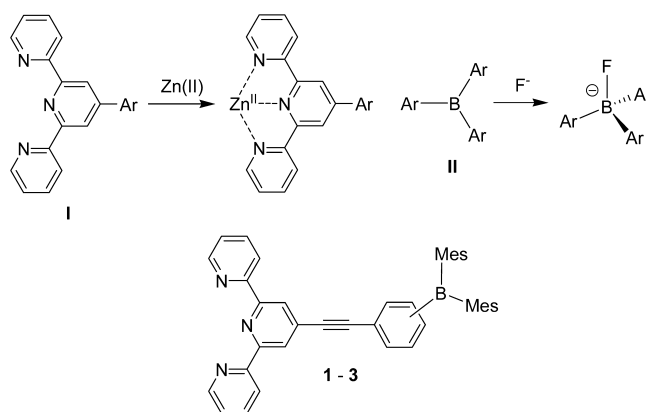
## INTRODUCTION

Molecular receptors capable of effectively recognizing charged or neutral species have been actively studied in the field of supramolecular chemistry, because such receptors can be utilized in sensing, catalysis, nanoscience, biomimicry, drug delivery, and separation science.<sup>1</sup> In the past several decades, as artificial cation receptors, a great number of acyclic and macrocyclic compounds have been reported and evaluated for their cation recognition ability.<sup>2</sup> At the same time, the design and construction of anion receptors have also attracted attention due to the increased importance of anions in physiological and environmental systems.<sup>3</sup> Although recognition of individual ionic species was successfully demonstrated by monotopic receptors, heteroditopic receptors that contain two disparate recognition sites for both cations and anions may also be good candidates for sensing purposes because they can exhibit enhanced affinity for target species in comparison to the corresponding monotopic receptors probably due to allosteric effects and favorable electrostatic interactions between the cobound ions in ion-pair receptors.<sup>4</sup>

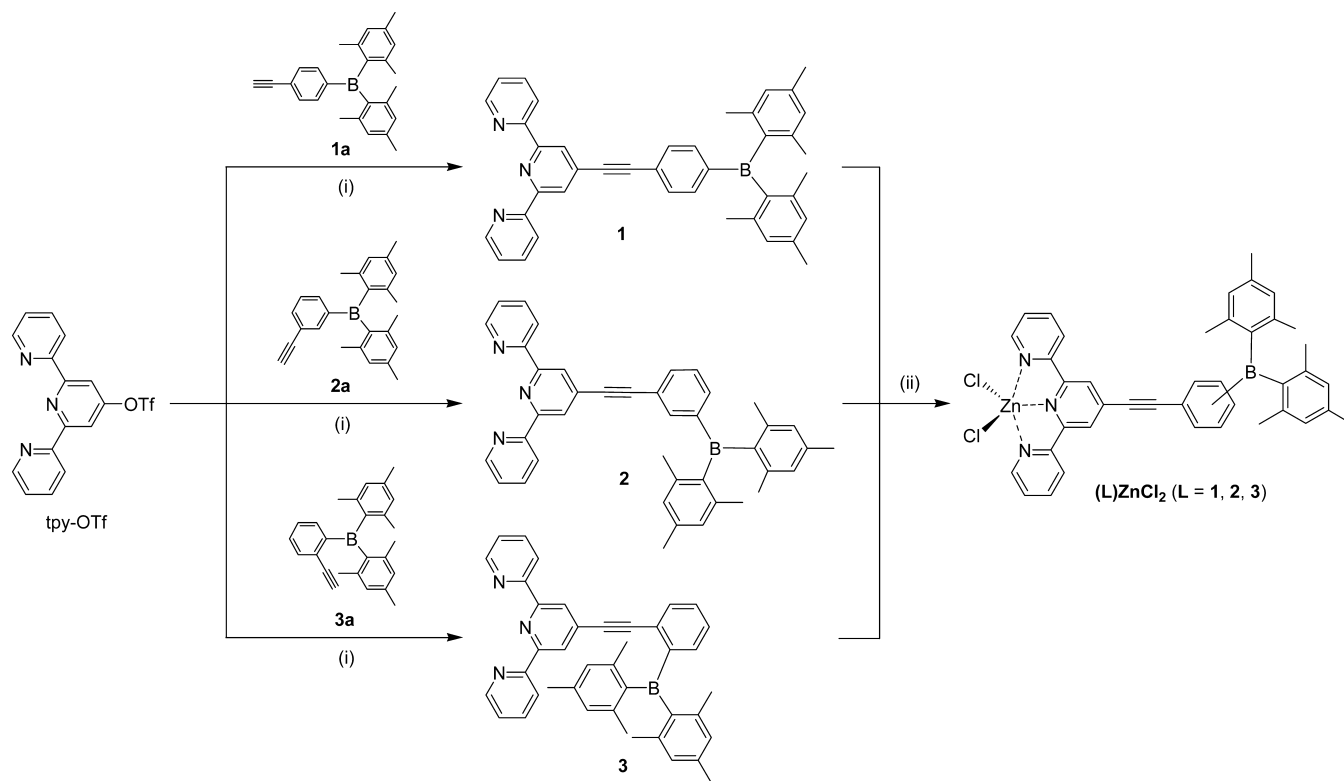
The terpyridine (2,2′:6′,2″-terpyridine) core has been extensively used as a metal ion receptor in coordination chemistry. Generally, terpyridine provides a tridentate N<sup>^</sup>N<sup>^</sup>N

binding site for metal ions and shows strong structural stability with fascinating electrochemical, photophysical, and photochemical properties (**I** in Chart 1).<sup>5</sup> In particular, when a metal

Chart 1



Received: November 26, 2013

Scheme 1. <sup>a</sup>

<sup>a</sup>Legend: (i) Pd(PPh<sub>3</sub>)<sub>4</sub>, CuI, *i*-Pr<sub>2</sub>NH, reflux, 49% (1), 36% (2), 57% (3); (ii) ZnCl<sub>2</sub>, CH<sub>3</sub>CN/CH<sub>2</sub>Cl<sub>2</sub> (1/1, v/v), 25 °C, 84% (1·ZnCl<sub>2</sub>), 95% (2·ZnCl<sub>2</sub>), 79% (3·ZnCl<sub>2</sub>).

ion with a  $d^{10}$  electron configuration (e.g., Zn(II) or Cd(II)) binds to a terpyridine with conjugated aryl substituents, especially at the 4'-position of the terpyridine core, efficient intramolecular charge transfer (ICT) from the substituted aryl donor to the metalated terpyridine acceptor takes place upon light excitation.<sup>6,7</sup> Since metal ion binding enhances the electron-accepting properties of terpyridine cores from aryl donors, it leads to a red shift of the ICT emission in comparison to the metal-unbound state. This effect has been used to detect and quantify various metal ions, including Zn(II).<sup>6,8,9</sup> On the other hand, triarylboranes have attracted significant attention as monotopic anion receptors due to their high Lewis acidity as well as high selectivity endowed by steric protection of the boron center with ortho substituents on the aryl group (II in Chart 1).<sup>10</sup> Upon anion binding to the boron center, the extended conjugation is disrupted by the population of the boron  $p_\pi$  orbital to give rise to changes in the absorption and/or emission intensity of triarylboranes. Indeed, triarylboranes have been utilized as effective and selective anion sensors to detect harmful anions such as fluoride and cyanide.<sup>11–17</sup>

While a number of multitopic receptors have been studied, ditopic receptors containing terpyridine and triarylborane for binding of both cationic metal ion and fluoride anion have been rarely reported. Note that Mes<sub>2</sub>B-functionalized N<sup>^</sup>N chelate compounds are known for binding Zn(II) or fluoride ions.<sup>18,19</sup> Instead, metal chelation effects on the Lewis acidity and optical properties of triarylboranes have been reported. For instance, Kitamura and co-workers demonstrated that the triarylborane-appended terpyridine complex [PtLCl]<sup>+</sup> (L = 4'-phenyl-(dimesitylboryl)-2,2':6',2''-terpyridine) shows synergistic effects of metal-to-ligand charge transfer (MLCT) and  $\pi(\text{aryl})-p_\pi(\text{B})$

CT interactions on the enhancement of MLCT absorption and emission due to effective conjugation between Pt(II)-terpyridine and arylborane units.<sup>20</sup> Wang and co-workers have reported a series of Mes<sub>2</sub>B-functionalized N<sup>^</sup>N,<sup>14,17,18,21,22</sup> N<sup>^</sup>C,<sup>12,22–24</sup> and N<sup>^</sup>C<sup>^</sup>N chelate<sup>25</sup> Pt(II) complexes. They showed that metal chelation not only enhances the fluoride binding affinity of boron centers but also alters phosphorescent properties that are useful in anion sensing<sup>16,17,24,26</sup> and OLED applications.<sup>25,27</sup>

Herein, we report a new series of ditopic terpyridine-terarylborane conjugates (1–3 in Chart 1) in which 4'-ethynylterpyridine is linked to the para, meta, and ortho positions of the phenyl ring of dimesitylphenylborane (Mes<sub>2</sub>PhB), respectively, to investigate dual complexation behavior toward Zn(II) cation and fluoride anion. The changes in optical properties of the conjugates with Zn(II) and/or fluoride binding were fully investigated by experimental and theoretical methods. The synthesis and crystal structures of corresponding Zn(II) complexes are also provided to understand the dual binding behavior of the conjugates.

## RESULTS AND DISCUSSION

**Synthesis and Characterization.** Three terpyridine-terarylborane conjugates (1–3) linked by an ethynylene group were synthesized by a palladium-catalyzed Sonogashira cross-coupling reaction between (ethynylphenyl)-dimesitylboryne (1a–3a) and 2,6-bis(pyridin-2-yl)pyridin-4-yl trifluoromethanesulfonate (tpy-OTf) (Scheme 1). To investigate the substitution position effect of the dimesitylboryl (Mes<sub>2</sub>B) group on the optical properties, as well as the effects of cation and anion binding, 4'-ethynylterpyridine was

introduced into the para, meta, and ortho positions of the phenyl ring of dimesitylphenylborane ( $\text{Mes}_2\text{PhB}$ ), respectively. The formation of conjugates **1–3** was characterized by multinuclear NMR spectroscopy and elemental analysis.  $^1\text{H}$  and  $^{13}\text{C}$  NMR spectra of **1–3** exhibit the expected resonances corresponding to mesityl and terpyridine moieties. Two singlets at  $\delta$  2.3 and 2.0 ppm assignable to the *p*- and *o*-methyl proton resonances of mesityl groups, respectively, indicate free rotation of the  $\text{Mes}_2\text{B}$  moiety in solution irrespective of its position on the phenyl group. The broad  $^{11}\text{B}$  NMR signals at  $\delta$  74–78 ppm confirm the presence of a trigonal-planar boron center. The reaction of each conjugate with zinc(II) chloride in mixed solvent ( $\text{CH}_3\text{CN}/\text{CH}_2\text{Cl}_2$ ) produced the corresponding Zn(II) complexes in high yield as white powders. The resulting complexes were also fully characterized by multinuclear NMR spectroscopy, elemental analysis, and single-crystal X-ray diffraction. Although the  $^{11}\text{B}$  NMR signals for all Zn(II) complexes were not observed, the apparent downfield chemical shifts of the proton resonances for the terpyridine group indicate binding of the Zn(II) center to terpyridine.<sup>28</sup> Finally, X-ray diffraction studies unequivocally revealed crystal structures for all Zn(II) complexes (Figure 1 and Table S2 (Supporting Information)). The structures show the formation of a 1:1 adduct ( $\text{L}\cdot\text{ZnCl}_2$ ,  $\text{L} = \mathbf{1–3}$ ) between  $\text{ZnCl}_2$  and terpyridine–triarylborane conjugate (**L**).<sup>8,29</sup> In all complexes, the zinc centers adopt a five-coordinate geometry with three nitrogen atoms and two chlorine atoms. Two chlorine atoms and one nitrogen atom of the central pyridine ring of the terpyridine moiety occupy equatorial positions, forming a distorted-trigonal-bipyramidal geometry around the zinc center. The equatorial Zn–N bond lengths are shorter than those of the axial Zn–N bonds in all complexes, as is typical for other terpyridine Zn(II) complexes (Table S2).<sup>8,29,30</sup> While the central pyridine and phenylene rings linked to the ethynylene group are substantially coplanar in  $\mathbf{1}\cdot\text{ZnCl}_2$  and  $\mathbf{2}\cdot\text{ZnCl}_2$  ( $\angle\text{pyd-Ph} = 15.1(2)^\circ$  for  $\mathbf{1}\cdot\text{ZnCl}_2$  and  $26.71(6)^\circ$  for  $\mathbf{2}\cdot\text{ZnCl}_2$ ), the two rings in  $\mathbf{3}\cdot\text{ZnCl}_2$  are perpendicularly oriented to each other ( $\angle\text{pyd-Ph} = 88.78(8)^\circ$ ). Inspection of the structure of  $\mathbf{3}\cdot\text{ZnCl}_2$  further shows that one mesityl ring plane is positioned right above the ethynylene–pyridine fragment and the two fragments are in a nearly parallel arrangement (Figure S1 (Supporting Information)). This feature indicates the presence of  $\pi$ – $\pi$  interactions between the two fragments. Indeed, interatomic distances between the mesityl carbon atoms and ethynylene–pyridine carbon atoms are very short (3.1–3.4 Å) (Figure S2 (Supporting Information)). The presence of  $\pi$ – $\pi$  interactions is also evidenced by the distortion of terpyridine fragment toward the mesityl ring, resulting in the deviation of the C25–C26–C27 bond angle from linearity ( $170.6(2)^\circ$ ) (Figure S1, left). Note that the angles for  $\mathbf{1}\cdot\text{ZnCl}_2$  and  $\mathbf{2}\cdot\text{ZnCl}_2$  are  $177.6(6)^\circ$  and  $176.26(15)^\circ$ , respectively.

To elucidate this structural feature in  $\mathbf{3}\cdot\text{ZnCl}_2$ , the crystal structure of conjugate **3** was determined (Figure 2). Remarkably, the terpyridine and phenylene rings are nearly coplanar ( $\angle\text{pyd-Ph} = 10.15(14)^\circ$ ) and the ethynylene linker is linearly connected to both rings in **3** ( $\angle\text{C25–C26–C27} = 177.0(3)^\circ$ ). This finding suggests that the observed  $\pi$ – $\pi$  interactions in  $\mathbf{3}\cdot\text{ZnCl}_2$  originate from an electronic source. Namely, the decreased electron density of the terpyridine moiety due to  $\text{ZnCl}_2$  binding likely facilitates  $\pi$ – $\pi$  interactions with the mesityl donor. It is also interesting to note that three nitrogen atoms of terpyridine in **3** are in a *cis,cis* conformation in the solid state. Finally, as observed in other triarylborane

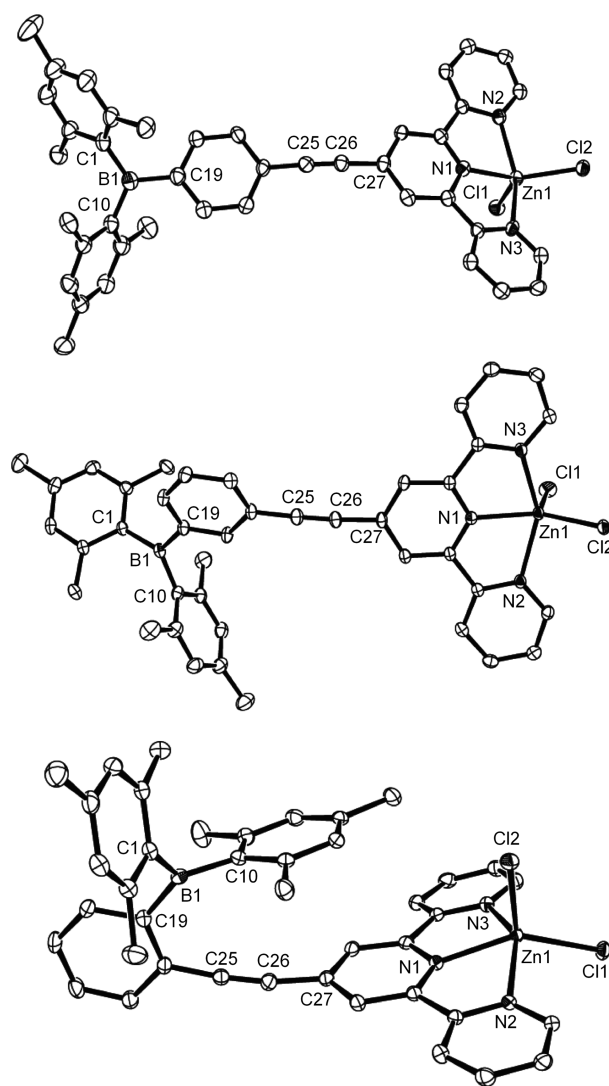


**Figure 1.** Crystal structures of  $\mathbf{1}\cdot\text{ZnCl}_2$  (top),  $\mathbf{2}\cdot\text{ZnCl}_2$  (middle), and  $\mathbf{3}\cdot\text{ZnCl}_2$  (bottom) (30% probability ellipsoids). H atoms and one  $\text{CH}_3\text{CN}$  molecule in  $\mathbf{1}\cdot\text{ZnCl}_2$  are omitted for clarity.

compounds, B(1) boron atoms adopt a trigonal-planar geometry ( $\sum\text{C–B–C} = 360^\circ$ ) in all Zn(II) complexes and in **3**.

**Absorption and Emission Properties.** The optical properties of conjugates **1–3** and their Zn(II) complexes were investigated in THF solution (Figure 3 and Table 1). The absorption spectra of **1–3** exhibit two major bands in the region of 250–375 nm. A lower energy absorption band appears in the energy order  $2 > 3 > 1$ . This is in parallel with the extent of conjugation between terpyridine and triarylborane groups, although the absorption edges in **1** and **3** are similar in energy. Zn(II) complexes of **1–3** also have absorption profiles similar to each other, and the lower energy absorption follows the same trend as for conjugates **1–3**. Interestingly, all absorption bands are slightly red-shifted in comparison to the respective absorption bands of conjugates, indicating a decrease in the band gap energy after Zn(II) complexation.

To gain insight into the electronic transitions of **1–3** and their Zn(II) complexes, TD-DFT calculations on the ground state ( $S_0$ ) optimized structures of all compounds were performed with the B3LYP functional and 6-31G(d) basis sets (Figure 4 and Table 2). Calculation results predict major

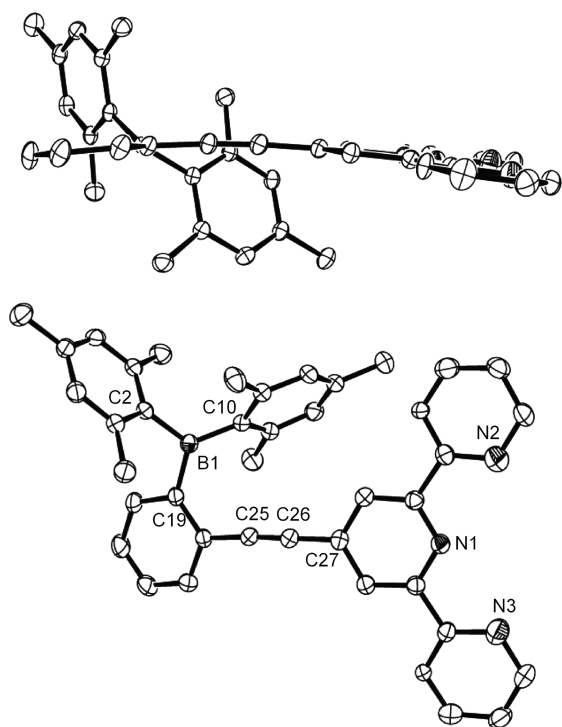


**Figure 2.** Side and top views of the crystal structure of **3** (30% probability ellipsoids). H atoms are omitted for clarity.

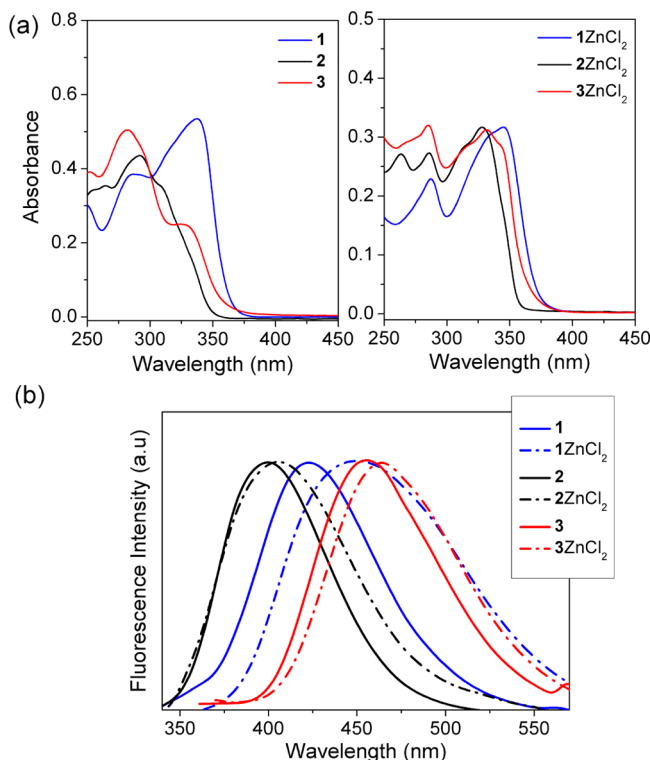


**Figure 3.** (a) UV/vis absorption and (b) fluorescence spectra of **1–3** and their Zn(II) complexes in THF ( $1.0 \times 10^{-5}$  M).

low-energy absorptions at 374, 356, and 363 nm for **1–3**, respectively, which is the same order as for experimentally observed absorption bands. While HOMOs are mainly located on both mesityl and phenylene–ethynylene moieties, the contribution from each fragment is observed differently. As the

**Table 1.** Optical Data for Conjugates **1–3** and Their Zn(II) Complexes

compound	$\lambda_{\text{abs}}/\text{nm}$ ( $\epsilon \times 10^{-3}/\text{M}^{-1} \text{cm}^{-1}$ ) <sup>a</sup>	$\lambda_{\text{ex}}/\text{nm}$ <sup>a</sup>	$\lambda_{\text{em}}/\text{nm}$ <sup>a</sup>	$\Phi_{\text{em}}$ <sup>a,b</sup>
<b>1</b>	250 (30.4), 285 (38.4), 338 (53.4)	281	424	0.19
<b>2</b>	253 (33.9), 265 (35.4), 293 (43.4), 310 (35.0)	294	398	0.08
<b>3</b>	282 (50.4), 295 (44.2), 325 (25.0)	284	454	0.03
<b>1</b> ·ZnCl <sub>2</sub>	288 (22.9), 346 (31.7)	335	450	0.15
<b>2</b> ·ZnCl <sub>2</sub>	264 (27.1), 286 (27.3), 328 (31.7)	328	408	0.07
<b>3</b> ·ZnCl <sub>2</sub>	286 (32.0), 332 (31.2), 344 (28.2)	332	465	0.03

<sup>a</sup>Measured in THF ( $1.0 \times 10^{-5}$  M). <sup>b</sup>Quinine sulfate as a standard (0.5 M H<sub>2</sub>SO<sub>4</sub>,  $\Phi = 0.55$ ).

conjugation length increases (**1** > **3** > **2**), contributions from the  $\pi$  orbital of the phenylene–ethynylene moiety become significant. It is notable that the HOMO of *m*-BMes<sub>2</sub>-substituted **2** is exclusively contributed by mesityl groups. Conversely, LUMOs are delocalized over each conjugate with a substantial contribution from the empty  $p_{\pi}(\text{B})$  orbital. These findings suggest that the lower energy absorption is mainly characterized by a  $\pi(\text{Ar}) \rightarrow p_{\pi}(\text{B})$  charge transfer (CT) transition where Ar is the mesityl and/or phenylene–ethynylene moiety. Significant contribution from a  $\pi \rightarrow p_{\pi}(\text{B})$  CT transition in **1–3** may be responsible for (i) the broad absorption feature (Figure 3a), (ii) the structureless emission profile (Figure 3b), (iii) the positive solvatochromism (Figure 5), and (iv) the gradual quenching of the lower energy absorption band upon fluoride binding to the boron atom (Figure 7). TD-DFT calculations on the ground state of Zn(II) complexes **1**·ZnCl<sub>2</sub>–**3**·ZnCl<sub>2</sub> predict major low energy absorptions at 404, 362, and 395 nm, respectively, similar to the trend in absorption spectra. The red-shifted absorption in Zn(II) complexes in comparison to the absorption in free conjugates is also consistent with experimental results. While the HOMOs have major contributions from mesityl groups, the LUMOs have substantial contributions from the central pyridine ring of terpyridine moieties. Contributions from the empty  $p_{\pi}(\text{B})$  orbital to LUMOs decrease in the order **1** > **3** > **2**. Thus, lower energy absorption in the Zn(II) complexes can be mainly assignable to a  $\pi(\text{Mes}) \rightarrow \pi^*(\text{Ar})$  (Ar = terpyridine–ethynylene) intramolecular CT (ICT) transition with slight  $\pi(\text{Mes}) \rightarrow p_{\pi}(\text{B})$  CT character. This result reflects the stabilization of the LUMO of the conjugate upon Zn(II) complexation. Consequently, the absorption energy of Zn(II) complexes decreases in comparison to that of free conjugates.

The photoluminescence (PL) spectra of conjugates **1–3** and their Zn(II) complexes display broad emission bands indicative of CT transition in nature (Figure 3b and Table 1).<sup>6,7</sup> The red-shifted emission bands for Zn(II) complexes in comparison with those of **1–3** are consistent with the absorption features. Among the pairs of conjugates and Zn(II) complexes, a red shift in the emission wavelength is most apparent for **1** and **1**·ZnCl<sub>2</sub> ( $\Delta\lambda_{\text{em}} = 26$  nm). It is notable that the emission energies of **3** and **3**·ZnCl<sub>2</sub> are considerably lower than those of **1** and **1**·ZnCl<sub>2</sub>, respectively. This finding is somewhat different from that observed in absorption spectra, in which the para-substituted **1** showed overall lower energy absorption than the ortho-substituted **3** (see TD-DFT results below).

Because the CT transition energy is largely affected by solvent polarity, the effect of solvent on the absorption and emission spectra of **1** and **3** was further examined. While both compounds exhibited low-energy absorption at nearly the same

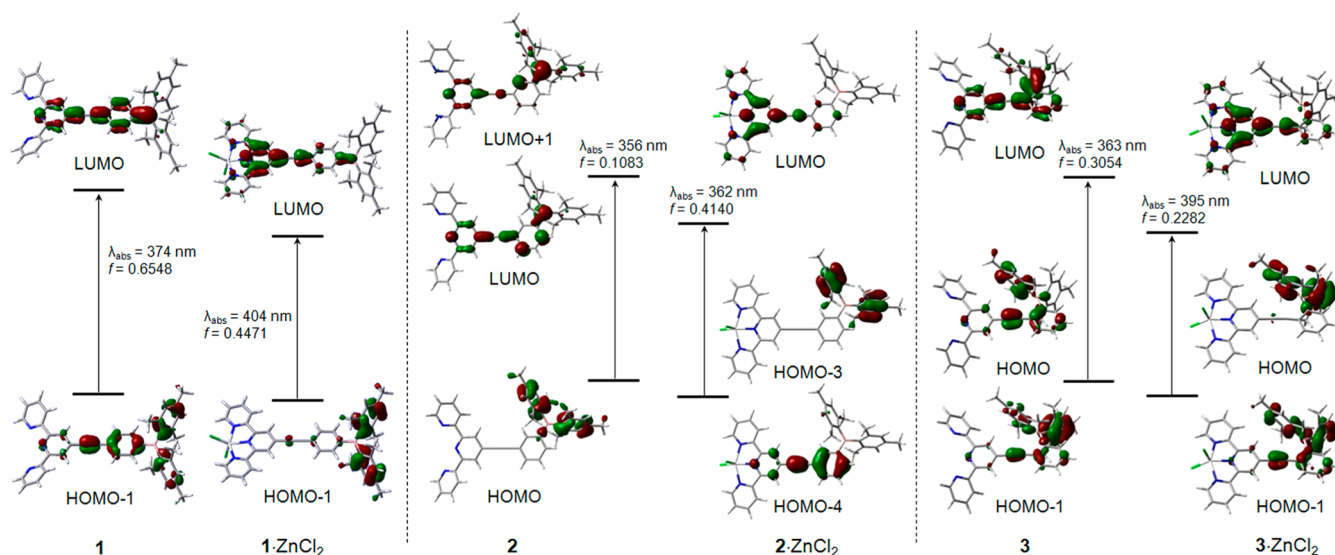


**Figure 4.** Molecular orbitals for 1–3 and 1·ZnCl<sub>2</sub>–3·ZnCl<sub>2</sub> at their ground state ( $S_0$ ) optimized geometries and lower energy electronic transitions from TD-DFT calculations (isovalue 0.04). Transition energies (in nm) were calculated using the TD-B3LYP method with 6-31G(d) basis sets.

**Table 2. Lower Energy Electronic Transitions for 1–3 and Their Zn(II) Complexes from TD-DFT Calculations<sup>a</sup>**

	state	$\lambda_{\text{calc}}$ /nm	$f$	assignment
1	$S_2$	373.9	0.6548	HOMO-1 → LUMO (90%)
2	$S_1$	356.1	0.1083	HOMO → LUMO (62%), HOMO → LUMO+1 (34%)
3	$S_2$	362.8	0.3054	HOMO-1 → LUMO (80%), HOMO → LUMO (10%)
1·ZnCl <sub>2</sub>	$S_2$	404.2	0.4471	HOMO-1 → LUMO (92%)
2·ZnCl <sub>2</sub>	$S_4$	361.7	0.4140	HOMO-3 → LUMO (56%), HOMO-4 → LUMO (30%)
3·ZnCl <sub>2</sub>	$S_2$	394.6	0.2282	HOMO-1 → LUMO (80%), HOMO → LUMO (12%)

<sup>a</sup>Singlet energies for the vertical transition calculated at the optimized  $S_0$  geometries.

wavelength in solvents with different polarities (Figure S3 (Supporting Information)), PL spectra clearly displayed positive solvatochromism, indicating the polar excited states of 1 and 3 (Figure 5). This result also indicates that emission is CT transition in nature. A red shift in the emission wavelength

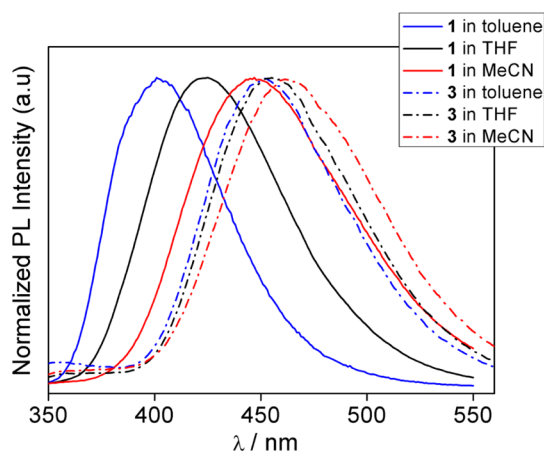


**Figure 5.** Normalized fluorescence spectra of 1 and 3 in different solvents.

upon increased solvent polarity is much more apparent for 1 ( $\Delta\lambda_{\text{em}} = 46$  nm for 1 and 10 nm for 3 between toluene and MeCN solutions), indicating that 1 has a more polar CT excited state than 3. Thus, 1 is expected to have a transition dipole moment greater than that of 3, which might be responsible for the higher molar absorption coefficient ( $\epsilon$ ) and quantum efficiency of 1 in comparison to those of 3.<sup>20</sup> Comparison of the emission bands of 1 and 3 in the same solvent shows that the emission energy of 3 is lower than that of 1 in all solvent systems. This result indicates that the lowest excited state of 3 should be lower in energy than that of 1. Since the absorption edge was very similar in energy for both compounds (Figure 3a), the lowest singlet excited state structures ( $S_1$ ) of 1 and 3 were optimized, and the transition energy was compared in detail (Figure 6). For both compounds, the lowest energy electronic transition is involved with a HOMO → LUMO transition (98% for 1 and 100% for 3) with substantial  $\pi \rightarrow p_{\pi}(\text{B})$  CT nature. Importantly, the transition energy of 3 (549 nm, 2.26 eV) is shown to be lower than that of 1 (492 nm, 2.52 eV), indicating a more stabilized  $S_1$  state for 3. Inspection of the  $S_1$  state structures of 1 and 3 reveals that while 1 has essentially identical  $S_1$  and  $S_0$  structures, 3 undergoes an apparent geometrical distortion in the  $S_1$  state. This is indicated by large distortion between pyridine and phenylene ring fragments ( $\angle_{\text{pyd-Ph}} = 15.4^\circ$  at  $S_0$  and  $37.3^\circ$  at  $S_1$  for 3) (Figure 6a). This result may suggest that the  $S_1$  state of 3 is more stabilized by geometrical changes, leading to lower emission energy. Furthermore, computation of the transition dipole moment ( $\mu$ ) and oscillator strength ( $f$ ) resulted in higher values for 1 than for 3 ( $\mu = 0.4058$  D and  $f = 0.0250$  for 1 and  $\mu = 0.1654$  D and  $f = 0.0092$  for 3). This result also supports that 1 exhibits significant solvatochromism and has higher quantum efficiency than 3.

**Cation and Anion Binding Studies.** To investigate the binding properties of 1–3 toward Zn(II) and fluoride ions, UV/vis absorption and fluorescence titration experiments were performed in THF. Titration results for 1 are shown in Figure 7, and the results for 2 and 3 are collected in Figures S4 and S5 (Supporting Information). The addition of incremental amounts of fluoride led to the gradual quenching of the lower energy absorption band at 338 nm, indicating that

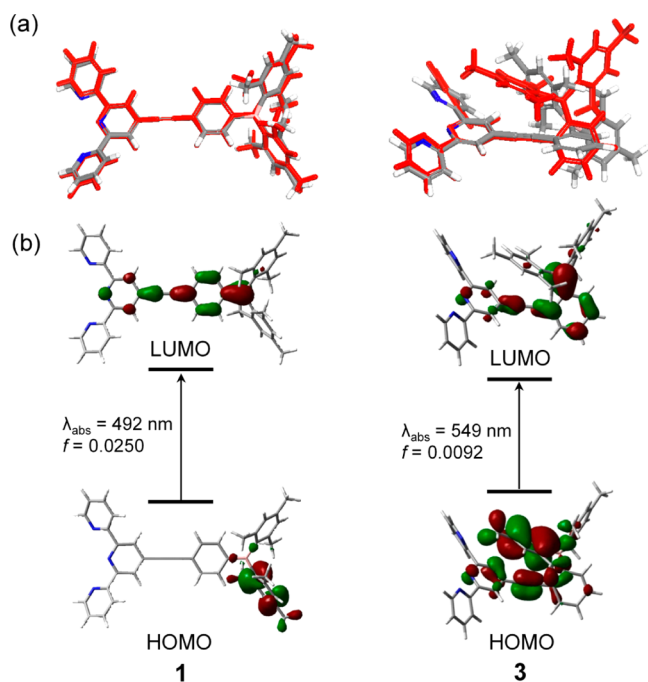


**Figure 6.** (a) Overlap of ground state ( $S_0$ , gray) and lowest excited state ( $S_1$ , red) optimized structures of 1 and 3. (b) Molecular orbitals for 1 and 3 at their  $S_1$  optimized geometries with the lowest energy electronic transition from TD-DFT calculations (isovalue 0.04).

fluoride binding to the boron center of 1 blocks the  $\pi \rightarrow p_\pi(\text{B})$  CT transition (Figure 7a).<sup>13,31</sup> Fitting of the absorbance data resulted in a high binding constant ( $K$ ) of ca.  $\sim 10^7 \text{ M}^{-1}$  in THF, which is comparable to values observed for triarylboranes with a  $\text{Mes}_2\text{PhB}$  group.<sup>15,32</sup> Similarly, the broad fluorescence band at 424 nm decreased in intensity upon fluoride addition while forming a new weak emission band at the higher energy region (ca. 360 nm). The structured band shape after fluoride binding suggests that emission of the fluoride adduct is attributable to a  $\pi-\pi^*$  transition in the phenylene-ethynylene-terpyridine fragment. Fluoride titration results for 2 and 3 showed similar quenching of both the lower energy absorption and fluorescence bands with the appearance of structured high-energy emission bands (Figure S4). Interestingly, while the  $K$  value of 2 is similar to that of 1, the  $K$  value of 3 is one order of magnitude lower than those of 1 and 2 (ca.  $1.0 \times 10^6 \text{ M}^{-1}$ , Table 3). This result can be ascribed to the steric hindrance of the ortho-substituted ethynyl group on the fluoride binding to the boron center in 3.

Next, the binding properties of 1–3 toward  $\text{ZnCl}_2$  were examined. Upon gradual addition of  $\text{ZnCl}_2$  to a solution of 1 ( $1.0 \times 10^{-5} \text{ M}$  in THF), the absorption band at 338 nm increased in intensity with a red shift (Figure 7b). The absorbance data, which were best fitted with a 1:1 binding isotherm, resulted in a  $K$  value of  $1.5 \times 10^6 \text{ M}^{-1}$ . The distinct isosbestic points at 286 and 326 nm also support 1:1 binding between 1 and  $\text{ZnCl}_2$ , in parallel with the crystal structure of 1· $\text{ZnCl}_2$ . The final absorption curve after  $\text{ZnCl}_2$  titrations was identical with that of 1· $\text{ZnCl}_2$ , as shown in Figure 3a. PL titrations exhibited similar quenching of the emission band with an apparent red shift upon  $\text{ZnCl}_2$  addition. The emission band shift accompanied an emission color change of the solution from deep blue to sky blue. Unlike the case with fluoride binding, the emission intensity after  $\text{ZnCl}_2$  binding remained

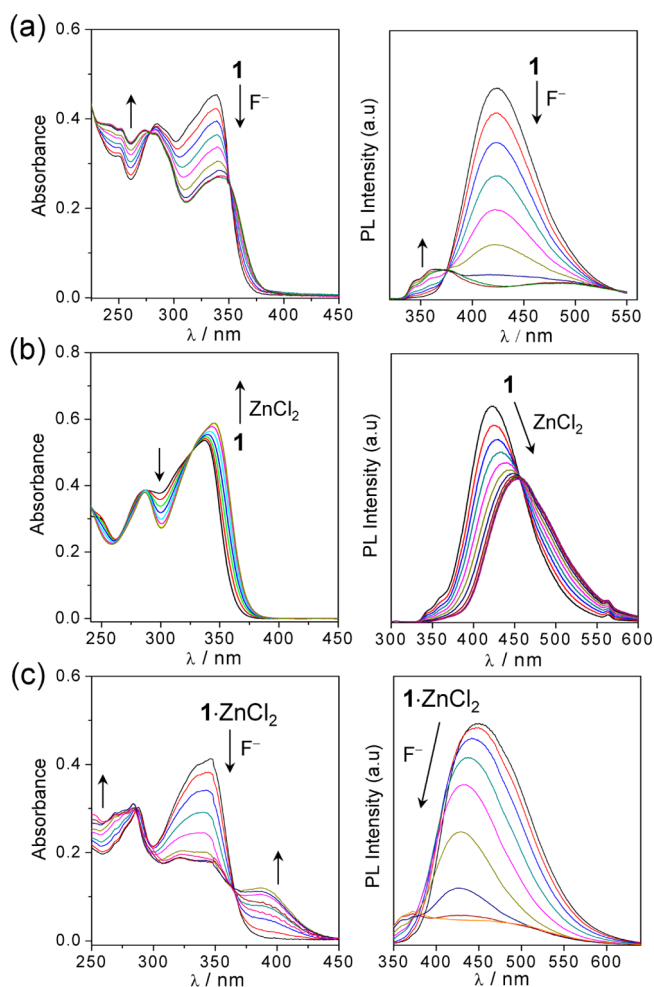


**Figure 7.** Spectral changes in UV/vis absorption and fluorescence of 1 ( $1.0 \times 10^{-5} \text{ M}$  in THF) upon addition of (a) TBAF ( $(0-1.5) \times 10^{-5} \text{ M}$  in THF) and (b)  $\text{ZnCl}_2$  ( $(0-2.4) \times 10^{-5} \text{ M}$  in  $\text{CH}_3\text{CN}$ ) and of 1· $\text{ZnCl}_2$  ( $1.0 \times 10^{-5} \text{ M}$  in THF) upon addition of (c) TBAF ( $(0-1.4) \times 10^{-5} \text{ M}$  in THF).

**Table 3. Binding Constants ( $K$ ) of Conjugates 1–3 and Their Zn(II) Complexes in THF**

compound	Zn(II) ( $\text{M}^{-1}$ )	$\text{F}^-$ ( $\text{M}^{-1}$ )
1	$1.5 \times 10^6$	$1.0 \times 10^7$
2	$5.0 \times 10^6$	$3.0 \times 10^7$
3	$5.0 \times 10^6$	$1.0 \times 10^6$
1· $\text{ZnCl}_2$		$5.0 \times 10^7$
2· $\text{ZnCl}_2$		$1.0 \times 10^7$
3· $\text{ZnCl}_2$		$4.0 \times 10^6$

relatively strong. This is consistent with the slightly lower quantum efficiency of 1· $\text{ZnCl}_2$  in comparison to that of 1 (Table 1). Similar absorption quenching with the appearance of a new lower energy band, as well as emission quenching with a red shift, was observed for 2 and 3 upon  $\text{ZnCl}_2$  addition (Figure S5 (Supporting Information)). This result indicates that both compounds have binding properties similar to those of 1 toward  $\text{ZnCl}_2$ . Compounds 2 and 3 also exhibited a level of high binding constants ( $K = 5.0 \times 10^6 \text{ M}^{-1}$ ) comparable with that of 1. This is a consequence of Zn(II) binding to the terpyridine moieties with a similar steric environment in all conjugates.

To examine the dual binding abilities of **1–3** toward Zn(II) and fluoride ions, fluoride titration experiments were further carried out with Zn(II) complexes  $1 \cdot \text{ZnCl}_2$ – $3 \cdot \text{ZnCl}_2$ . As shown in Figure 7c, the addition of fluoride to the solution of  $1 \cdot \text{ZnCl}_2$  led to gradual quenching of the low-energy absorption band at 346 nm along with formation of a new lower energy band at 390 nm with a distinct isosbestic point at 365 nm. This result indicates fluoride binding to the boron center of  $1 \cdot \text{ZnCl}_2$ . A high fluoride binding constant of ca.  $5.0 \times 10^7 \text{ M}^{-1}$  was also estimated. Complexes  $2 \cdot \text{ZnCl}_2$  and  $3 \cdot \text{ZnCl}_2$  showed similar absorption changes upon fluoride binding (Figure S6 (Supporting Information)). Although the estimated fluoride binding constant of  $3 \cdot \text{ZnCl}_2$  ( $K = 4.0 \times 10^6 \text{ M}^{-1}$ ) was still lower than those of  $1 \cdot \text{ZnCl}_2$  and  $2 \cdot \text{ZnCl}_2$  ( $K = \text{ca.} >10^7 \text{ M}^{-1}$ ) due to steric effects, it was higher than that of free conjugate **3** ( $K = 1.0 \times 10^6 \text{ M}^{-1}$ ). The increased  $K$  value for  $3 \cdot \text{ZnCl}_2$  strongly indicates that the Lewis acidity of a boron center was enhanced by Zn(II) complexation.<sup>17</sup> It is worth mentioning that the high binding constants of  $>10^7 \text{ M}^{-1}$  obtained by fitting are difficult to compare accurately. Furthermore, it is known that Zn(II) centers in bipyridine complexes are susceptible to fluoride ions.<sup>18</sup> However, as shown in Figure 7 and Figure S6 (Supporting Information), the present terpyridine–Zn(II) complexes did not show abnormal spectral changes up to 2 equiv of fluoride addition, indicating relatively high stability. <sup>1</sup>H NMR titration results of  $1 \cdot \text{ZnCl}_2$  also support the preferential binding of fluoride to the boron center (Figure S7 (Supporting Information)). After full binding of fluoride to the boron center, however, excess fluoride addition caused dissociation of Zn(II) centers. While PL titrations of  $1 \cdot \text{ZnCl}_2$  exhibited quenching of the emission band at 450 nm, the band was gradually blue-shifted upon fluoride binding. It finally became a weak structured emission centered at 370 nm with a broad tail to 600 nm (Figure 7c). The structured emission may indicate that the  $\pi$ – $\pi^*$  transition in the phenylene–ethynylene–terpyridine fragment is a dominant emission process in the fluoride adduct, although the broad emission might be due to the newly formed lower energy CT state caused by elevation of  $\pi(\text{Mes})$  level upon fluoride binding, as observed in the absorption titrations above. As a result, the sky blue emission color of the solution of  $1 \cdot \text{ZnCl}_2$  almost disappeared at the end of titrations. Similar emission changes were also observed for  $2 \cdot \text{ZnCl}_2$  and  $3 \cdot \text{ZnCl}_2$  with an apparent increase in the emission intensity of high-energy bands (Figure S6 (Supporting Information)).

On the basis of the titration results of conjugates **1–3** and their Zn(II) complexes toward  $\text{ZnCl}_2$  and/or fluoride, we finally tested the conjugates as dual receptors for Zn(II) cation and fluoride anion. The absorption and fluorescence changes of **1–3** were examined upon sequential addition of  $\text{ZnCl}_2$  and fluoride (Figure 8 and Figure S8 (Supporting Information)). As shown in Figure 8, the absorption and emission bands of **1** underwent red shifts upon addition of  $\text{ZnCl}_2$ , with an emission color change from deep blue to sky blue. The subsequent addition of fluoride into the solution led to gradual quenching of both the absorption and emission bands with the growth of a new lower energy absorption band accompanied by disappearance of the emission color. In fact, this experiment reproduced the results of previous binding studies of **1** with  $\text{ZnCl}_2$  and of  $1 \cdot \text{ZnCl}_2$  with fluoride. Conjugates **2** and **3** also showed similar in situ binding behavior (Figure S8 (Supporting Information)). Therefore, the terpyridine–triarylborane conjugates **1–3** could

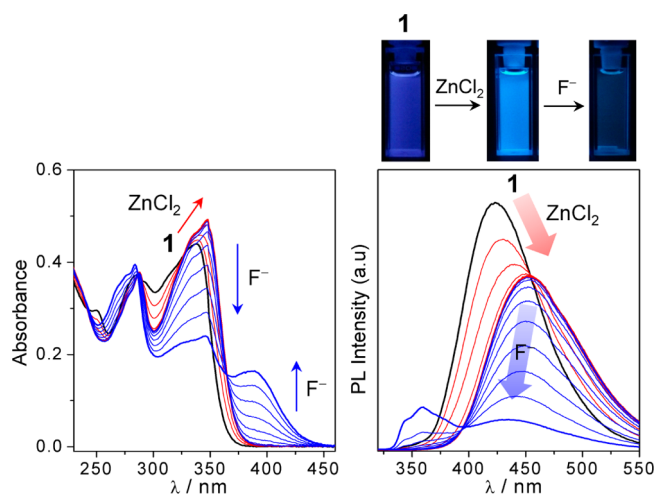


**Figure 8.** Spectral changes in UV/vis absorption (left) and fluorescence (right) of **1** ( $1.0 \times 10^{-5} \text{ M}$  in THF) upon sequential addition of  $\text{ZnCl}_2$  (red curves, 0–2.0 equiv) and TBAF (blue curves, 0–1.5 equiv). The pictures show the emission color change of a solution of **1** under UV illumination upon sequential addition of  $\text{ZnCl}_2$  and TBAF.

be potentially useful for sensing both Zn(II) cation and fluoride anion, as well as each ionic species.

## CONCLUSION

Ditopic terpyridine–triarylborane conjugates (**1–3**) and their Zn(II) complexes were prepared and characterized to investigate the dual complexation behavior of conjugates toward Zn(II) cation and fluoride anion. Experimental and theoretical studies showed that the  $\pi(\text{Ar}) \rightarrow p_r(\text{B})$  ( $\text{Ar} = \text{Mes}$  and/or phenylene–ethynylene) charge transfer (CT) transition in **1–3** switched to  $\pi(\text{Mes}) \rightarrow \pi^*(\text{Ar})$  ( $\text{Ar} = \text{terpyridine}$ –ethynylene) intramolecular CT in the Zn(II) complexes, resulting in red shifts of both the absorption and emission bands in comparison to those of the free conjugates. UV/vis absorption and fluorescence titration experiments of **1–3** exhibited gradual quenching of the absorption and fluorescence bands upon addition of fluoride, while the addition of  $\text{ZnCl}_2$  gave rise to red shifts of both bands. The fluoride titrations of Zn(II) complexes also led to quenching of both the absorption and emission bands. Finally, sequential addition of  $\text{ZnCl}_2$  and fluoride to the conjugates caused an emission color change from deep blue to sky blue to dark. This suggests that the conjugates are potentially useful as dual receptors for Zn(II) cation and fluoride anion.

## EXPERIMENTAL SECTION

**General Considerations.** All operations were performed under an inert nitrogen atmosphere using standard Schlenk and glovebox techniques. Anhydrous grade solvents (Aldrich) were dried by passing them through an activated alumina column and stored over activated molecular sieves (5 Å). Spectrophotometric grade THF and  $\text{CH}_3\text{CN}$  (Merck) were used for absorption and emission measurements. Commercial reagents were used as obtained without any further purification from Aldrich (*n*-BuLi (2.5 M solution in *n*-hexanes), tetra-*n*-butylammonium fluoride (TBAF), diisopropylamine (*i*-Pr<sub>2</sub>NH), Pd(PPh<sub>3</sub>)<sub>4</sub>, CuI, dimesitylboron fluoride (Mes<sub>2</sub>BF), sodium hydroxide, sodium carbonate,  $\text{ZnCl}_2$ ), TCI (1-bromo-4-iodobenzene, 1-bromo-3-iodobenzene, 1-bromo-2-iodobenzene), and Alfa Aesar ((trimethylsilyl)acetylene), (4-Ethynylphenyl)dimesitylborane (**1a**),<sup>33</sup> (2-(3-bromophenyl)ethynyl)trimethylsilane,<sup>34</sup> (2-ethynylphenyl)-

dimesitylborane (**3a**),<sup>35</sup> and 2,6-bis(pyridin-2-yl)pyridin-4-yl trifluoromethanesulfonate (tpy-OTf)<sup>36</sup> were synthesized according to the reported procedures. Deuterated solvents from Cambridge Isotope Laboratories were used. NMR spectra were recorded on a Bruker 300 AM spectrometer (300.13 MHz for <sup>1</sup>H, 75.48 MHz for <sup>13</sup>C, 96.29 MHz for <sup>11</sup>B) at ambient temperature. Chemical shifts are given in ppm and are referenced against external Me<sub>4</sub>Si (<sup>1</sup>H, <sup>13</sup>C) and BF<sub>3</sub>·OEt<sub>2</sub> (<sup>11</sup>B). Elemental analyses were performed on an EA1110 (FISONS Instruments) by the Environmental Analysis Laboratory at KAIST. Melting (mp) or decomposition points (dec pt) of solid compounds were measured using a MEL-TEMP II instrument (Laboratory Devices, Inc.). UV/vis absorption and PL spectra were recorded on a Varian Cary 100 and a HORIBA FluoroMax-4P spectrophotometers, respectively.

**Synthesis of 2-(4-(2-(4-(Dimesitylboryl)phenyl)ethynyl)-6-(pyridin-2-yl)pyridin-2-yl)pyridine (1).** In a Schlenk flask charged with tpy-OTf (0.50 g, 1.31 mmol), (4-ethynylphenyl)-dimesitylborane (**1a**; 0.50 g, 1.44 mmol), Pd(PPh<sub>3</sub>)<sub>4</sub> (30 mg, 0.026 mmol), and CuI (5 mg, 0.026 mmol) was added 30 mL of anhydrous diisopropylamine under a nitrogen atmosphere, and the reaction mixture was heated at reflux for 24 h. After it was cooled to room temperature, the resulting dark brown solution was concentrated and purified by silica gel column chromatography (eluent: ethyl acetate/*n*-hexane 1/4) to give a white powder of **1** (0.37 g, 49%). <sup>1</sup>H NMR (CDCl<sub>3</sub>): δ 8.77 (dq, *J* = 4.8, 0.8 Hz, 2H, Py-H), 8.67 (dt, *J* = 8.0, 0.9 Hz, 2H, Py-H), 8.62 (s, 2H, Py-H), 7.93 (td, *J* = 7.7, 1.8 Hz, 2H, Py-H), 7.57 (d, *J* = 1.5 Hz, 4H, Ph-H), 7.41 (m, 2H, Py-H), 6.87 (s, 4H, Mes-H), 2.30 (s, 6H, Mes-CH<sub>3</sub>), 2.05 (s, 12H, Mes-CH<sub>3</sub>). <sup>13</sup>C NMR (CDCl<sub>3</sub>): δ 155.51, 155.46, 149.12, 140.86, 138.96, 137.10, 136.09, 133.27, 131.45, 128.28, 125.60, 124.11, 122.97, 121.33 (Ar-C), 94.05, 89.29 (ethynylene-C), 23.48, 21.27 (Mes-CH<sub>3</sub>). <sup>11</sup>B NMR (CDCl<sub>3</sub>): δ 78 (br). Mp: 226 °C. Anal. Calcd for C<sub>41</sub>H<sub>36</sub>BN<sub>3</sub>: C, 84.68; H, 6.24; N, 7.23. Found: C, 84.80; H, 6.21; N, 7.26.

**Synthesis of (3-Ethynylphenyl)dimesitylborane (2a).** To a solution of (2-(3-bromophenyl)ethynyl)trimethylsilane (0.50 g, 2.0 mmol) in dry THF (20 mL) was added *n*-BuLi (10 mL, 2.0 mmol) dropwise at -78 °C. After it was stirred for 1 h at this temperature, a THF solution (5 mL) of Mes<sub>2</sub>BF (0.54 g, 2.0 mmol) was slowly added to the mixture. The reaction mixture was stirred for 1 h at -78 °C and then gradually warmed to room temperature. After it was stirred overnight, the mixture was quenched by the addition of saturated aqueous NH<sub>4</sub>Cl (30 mL). The organic layer was separated, and the aqueous layer was extracted with Et<sub>2</sub>O (3 × 30 mL). The combined organic layers were dried over MgSO<sub>4</sub>, filtered, and concentrated under reduced pressure. The crude product was purified by silica gel column chromatography (eluent: *n*-hexane) to yield dimesityl(3-(2-(trimethylsilyl)ethynyl)phenyl)borane (**2b**) as a white powder (0.55 g, 65%). <sup>1</sup>H NMR (CDCl<sub>3</sub>): δ 7.62 (s, 1H, Ph-H), 7.58 (dt, *J* = 7.6, 1.5 Hz, 1H, Ph-H), 7.43 (dt, *J* = 7.5, 1.3 Hz, 1H, Ph-H), 7.29 (t, *J* = 7.6 Hz, 1H, Ph-H), 6.80 (s, 4H, Mes-H), 2.30 (s, 6H, Mes-CH<sub>3</sub>), 1.96 (s, 12H, Mes-CH<sub>3</sub>), 0.21 (s, 9H, TMS-CH<sub>3</sub>).

Next, **2b** (0.30 g, 0.71 mmol) was dissolved in THF (10 mL) and treated with TBAF (ca. 1.0 M in THF, 5 mL). After the mixture was stirred for 1 h at room temperature, aqueous HCl (ca. 3.0 M, 10 mL) was added and the mixture stirred for 0.5 h. The resulting solution was extracted with diethyl ether (10 mL), and the organic portions were washed with water (3 × 10 mL). The combined organic layers were dried over MgSO<sub>4</sub>, filtered, and dried under reduced pressure. The solid mixture obtained was purified by silica gel column chromatography (eluent: *n*-hexane) to give a white powder of **2a** (0.23 g, 92%). <sup>1</sup>H NMR (CDCl<sub>3</sub>): δ 7.58 (s, 1H, Ph-H), 7.54 (dt, *J* = 7.7, 1.4 Hz, 1H, Ph-H), 7.42 (dt, *J* = 7.5, 1.3 Hz, 1H, Ph-H), 7.27 (td, *J* = 7.6, 0.6 Hz, 1H, Ph-H), 6.75 (s, 4H, Mes-H), 2.96 (s, 1H, ethynyl-H), 2.24 (s, 6H, Mes-CH<sub>3</sub>), 1.91 (s, 12H, Mes-CH<sub>3</sub>). <sup>13</sup>C NMR (CDCl<sub>3</sub>): δ 141.80, 140.23, 139.95, 137.39, 136.27, 129.29, 129.04, 122.85 (Ar-C), 84.86, 78.22 (ethynyl-C), 24.43, 22.24 (Mes-CH<sub>3</sub>). <sup>11</sup>B NMR (CDCl<sub>3</sub>): δ 74 (br). Anal. Calcd for C<sub>26</sub>H<sub>27</sub>B: C, 89.15; H, 7.77. Found: C, 88.70; H, 7.86.

**Synthesis of 2-(4-(2-(3-(Dimesitylboryl)phenyl)ethynyl)-6-(pyridin-2-yl)pyridin-2-yl)pyridine (2).** A procedure analogous to

that for **1** was employed with tpy-OTf (0.33 g, 0.86 mmol) and **2a** (0.33 g, 0.87 mmol) to afford a white powder of **2** (0.18 g, 36%). <sup>1</sup>H NMR (CDCl<sub>3</sub>): δ 8.76 (d, *J* = 4.2 Hz, 2H, Py-H), 8.67 (d, *J* = 8.0 Hz, 2H, Py-H), 8.57 (s, 2H, Py-H), 7.94 (td, *J* = 7.7, 1.6 Hz, 2H, Py-H), 7.74 (s, 1H, Ph-H), 7.71 (dt, *J* = 7.6, 1.5 Hz, 1H, Ph-H), 7.56 (dt, *J* = 7.5, 1.2 Hz, 1H, Ph-H), 7.43 (m, 3H, Py-H and Ph-H), 6.87 (s, 4H, Me-H), 2.36 (s, 6H, Mes-CH<sub>3</sub>), 2.05 (s, 12H, Mes-CH<sub>3</sub>). <sup>13</sup>C NMR (CDCl<sub>3</sub>): δ 156.54, 156.37, 150.09, 141.76, 140.36, 139.94, 137.93, 137.60, 135.99, 134.38, 129.35, 129.18, 124.98, 123.78, 123.19, 122.20 (Ar-C), 95.01, 88.48 (ethynylene-C), 24.44, 22.25 (Mes-CH<sub>3</sub>). <sup>11</sup>B NMR (CDCl<sub>3</sub>): δ 74 (br). Mp: 240 °C. Anal. Calcd for C<sub>41</sub>H<sub>36</sub>BN<sub>3</sub>: C, 84.68; H, 6.24; N, 7.23. Found: C, 84.16; H, 6.28; N, 6.99.

**Synthesis of 2-(4-(2-(2-(Dimesitylboryl)phenyl)ethynyl)-6-(pyridin-2-yl)pyridin-2-yl)pyridine (3).** A procedure analogous to that for **1** was employed with tpy-OTf (0.40 g, 1.05 mmol) and **3a** (0.45 g, 1.28 mmol) to afford a white powder of **3** (0.35 g, 57%). Single crystals suitable for an X-ray diffraction study were obtained by slow evaporation of a CH<sub>2</sub>Cl<sub>2</sub> solution of **3**, giving colorless blocklike crystals. <sup>1</sup>H NMR (CDCl<sub>3</sub>): δ 8.80 (d, *J* = 4.5 Hz, 2H, Py-H), 8.64 (d, *J* = 7.9 Hz, 2H, Py-H), 8.18 (s, 2H, Py-H), 7.94 (td, *J* = 8.0, 1.3 Hz, 2H, Py-H), 7.63 (dt, *J* = 7.6, 0.8 Hz, 2H, Ph-H), 7.48 (m, 1H, Ph-H), 7.42 (m, 2H, Py-H), 7.36 (d, *J* = 0.8 Hz, 1H, Ph-H), 7.34 (m, 1H, Ph-H), 6.82 (s, 4H, Mes-H), 2.21 (s, 6H, Mes-CH<sub>3</sub>), 2.07 (s, 12H, Mes-CH<sub>3</sub>). <sup>13</sup>C NMR (CDCl<sub>3</sub>): δ 156.81, 156.08, 150.07, 141.72, 140.20, 137.77, 135.28, 134.46, 134.17, 131.24, 129.42, 127.25, 124.81, 123.95, 122.09 (Ar-C), 95.18, 91.32 (ethynylene-C), 24.19, 22.16 (Mes-CH<sub>3</sub>). <sup>11</sup>B NMR (CDCl<sub>3</sub>): δ 76 (br). Mp: 208 °C. Anal. Calcd for C<sub>41</sub>H<sub>36</sub>BN<sub>3</sub>: C, 84.68; H, 6.24; N, 7.23. Found: C, 84.32; H, 6.26; N, 7.25.

**Synthesis of 1·ZnCl<sub>2</sub>.** To a solution of **1** (50 mg, 0.086 mmol) in CH<sub>2</sub>Cl<sub>2</sub>/CH<sub>3</sub>CN (1/1, v/v, 10 mL) was added ZnCl<sub>2</sub> (15 mg, 0.11 mmol) in CH<sub>3</sub>CN (3 mL). After the mixture was stirred for 2 h at room temperature, the solvent was evaporated off under reduced pressure and the resulting white powder was washed with CH<sub>3</sub>CN and dried under vacuum at room temperature (52 mg, 84%). Single crystals suitable for an X-ray diffraction study were obtained by slow evaporation of a DMF/CH<sub>3</sub>CN solution of 1·ZnCl<sub>2</sub>, giving colorless needlelike crystals. <sup>1</sup>H NMR (CDCl<sub>3</sub>): δ 9.13 (dq, *J* = 4.9, 0.7 Hz, 2H, Py-H), 8.27 (s, 2H, Py-H), 8.17 (d, *J* = 8.0 Hz, 2H, Py-H), 7.94 (td, *J* = 7.7, 1.7 Hz, 2H, Py-H), 7.59 (m, 6H, Py-H and Ph-H), 6.89 (s, 4H, Mes-H), 2.36 (s, 6H, Mes-CH<sub>3</sub>), 2.05 (s, 12H, Mes-CH<sub>3</sub>). <sup>13</sup>C NMR (CDCl<sub>3</sub>): δ 151.08, 150.37, 147.41, 142.26, 141.74, 140.54, 140.29, 138.88, 136.89, 132.78, 129.36, 128.20, 124.47, 124.15, 122.02 (Ar-C), 100.50, 87.91 (ethynylene-C), 24.44, 22.22 (Mes-CH<sub>3</sub>). <sup>11</sup>B signal was not observed. Dec pt: 246 °C. Anal. Calcd for C<sub>41</sub>H<sub>36</sub>BCl<sub>2</sub>N<sub>3</sub>Zn: C, 68.60; H, 5.05; N, 5.85. Found: C, 68.00; H, 4.98; N, 5.98.

**Synthesis of 2·ZnCl<sub>2</sub>.** A procedure analogous to that for 1·ZnCl<sub>2</sub> was employed with **2** (40 mg, 0.069 mmol) and ZnCl<sub>2</sub> (10 mg, 0.073 mmol) to afford a white powder (47 mg, 95%) of 2·ZnCl<sub>2</sub>. Single crystals suitable for an X-ray diffraction study were obtained by slow evaporation of a MeOH/CH<sub>2</sub>Cl<sub>2</sub> solution of 2·ZnCl<sub>2</sub>, giving colorless rodlike crystals. <sup>1</sup>H NMR (CDCl<sub>3</sub>): δ 9.18 (dq, *J* = 5.0, 0.8 Hz, 2H, Py-H), 8.30 (s, 2H, Py-H), 8.20 (dt, *J* = 8.0, 0.8 Hz, 2H, Py-H), 8.06 (td, *J* = 7.7, 1.7 Hz, 2H, Py-H), 7.83 (s, 1H, Ph-H), 7.76 (dt, 7.7, 1.4 Hz, 1H, Ph-H), 7.70 (dd, *J* = 5.0, 2.8 Hz, 1H, Py-H), 7.68 (dd, *J* = 5.0, 1.0 Hz, 1H, Py-H), 7.65 (dt, *J* = 7.4, 1.4 Hz, 1H, Ph-H), 7.49 (t, *J* = 7.5 Hz, 1H, Py-H), 6.89 (s, 4H, Mes-H), 2.37 (s, 6H, Mes-CH<sub>3</sub>), 2.05 (s, 12H, Mes-CH<sub>3</sub>). <sup>13</sup>C NMR (CDCl<sub>3</sub>): δ 151.13, 150.36, 147.53, 141.87, 140.58, 140.26, 140.19, 139.13, 138.85, 136.58, 129.55, 129.37, 128.21, 124.09, 121.94, 121.58 (Ar-C), 100.67, 86.69 (ethynylene-C), 24.46, 22.24 (Mes-CH<sub>3</sub>). <sup>11</sup>B signal was not observed. Dec pt: 232 °C. Anal. Calcd for C<sub>41</sub>H<sub>36</sub>BCl<sub>2</sub>N<sub>3</sub>Zn: C, 68.60; H, 5.05; N, 5.85. Found: C, 68.53; H, 5.26; N, 6.17.

**Synthesis of 3·ZnCl<sub>2</sub>.** A procedure analogous to that for 1·ZnCl<sub>2</sub> was employed with **3** (38 mg, 0.065 mmol) and ZnCl<sub>2</sub> (10 mg, 0.073 mmol) to afford a greenish yellow powder (37 mg, 79%) of 3·ZnCl<sub>2</sub>. Single crystals suitable for an X-ray diffraction study were obtained by slow evaporation of a CH<sub>3</sub>CN/CH<sub>2</sub>Cl<sub>2</sub> solution of 3·ZnCl<sub>2</sub>, giving colorless rodlike crystals. <sup>1</sup>H NMR (CDCl<sub>3</sub>): δ 9.18 (dt, *J* = 4.8, 1.2 Hz, 2H, Py-H), 8.14 (m, 4H, Py-H), 7.77 (s, 2H, Py-H), 7.74 (m, 3H,

Py-H and Ph-H), 7.57 (td,  $J = 7.1, 1.8$  Hz, 1H, Ph-H), 7.49 (td,  $J = 7.7, 1.4$  Hz, 1H, Ph-H), 7.43 (m, 1H, Ph-H), 6.85 (s, 4H, Mes-H), 2.28 (s, 6H, Mes-CH<sub>3</sub>), 2.05 (s, 12H, Mes-CH<sub>3</sub>). <sup>13</sup>C NMR (CDCl<sub>3</sub>):  $\delta$  151.19, 150.04, 147.67, 142.04, 140.55, 140.39, 139.33, 135.85, 134.64, 131.74, 131.01, 129.37, 128.26, 125.41, 123.97, 121.71 (Ar-C), 100.96, 86.11 (ethynylene-C), 24.27, 22.38 (Mes-CH<sub>3</sub>). <sup>11</sup>B signal was not observed. Dec pt: >300 °C. Anal. Calcd for C<sub>41</sub>H<sub>36</sub>BCl<sub>2</sub>N<sub>3</sub>Zn: C, 68.60; H, 5.05; N, 5.85. Found: C, 68.54; H, 5.02; N, 5.95.

**UV/Vis Absorption and PL Measurements.** UV/vis and PL measurements were performed with a 1 cm quartz cuvette at ambient temperature. A solution of conjugate or Zn(II) complex (3.0 mL,  $1 \times 10^{-5}$  M) was titrated with incremental amounts of ZnCl<sub>2</sub> in CH<sub>3</sub>CN or TBAF in THF ( $\sim 10^{-3}$  M). The absorbance data obtained were fitted to a 1:1 binding isotherm to estimate a binding constant ( $K$ ). Detailed conditions are given in the figure captions. Quantum efficiencies of compounds were measured with reference to that of quinine sulfate (0.5 M H<sub>2</sub>SO<sub>4</sub>,  $\Phi = 0.55$ ).<sup>37</sup>

**X-ray Crystallography.** Single crystals of all compounds were coated with Paratone-N oil, and the diffraction was measured at 100 K. The crystallographic measurements of [1·ZnCl<sub>2</sub>](MeCN) and 2·ZnCl<sub>2</sub> were performed by synchrotron radiation ( $\lambda = 0.62988$  Å) on a ADSC Quantum-210 detector at 2D SMC with a silicon (111) double-crystal monochromator (DCM) at the Pohang Accelerator Laboratory, Pohang, Korea. The ADSC Q210 ADX program<sup>38</sup> was used for data collection, and HKL3000sm (Ver. 703r)<sup>39</sup> was used for cell refinement, reduction, and absorption correction. The crystallographic measurements of crystals of 3 and 3·ZnCl<sub>2</sub> were performed on a Bruker SMART Apex II CCD area detector diffractometer with graphite-monochromated Mo K $\alpha$  radiation ( $\lambda = 0.71073$  Å). The crystal structures were solved by direct methods<sup>40</sup> and refined by full-matrix least-squares refinement with SHELXL-97<sup>41</sup> or SHELXL-2013.<sup>42</sup> The positions of all non-hydrogen atoms were refined with anisotropic displacement factors. All hydrogen atoms were placed using a riding model, and their positions were constrained relative to their parent atoms using the appropriate HFIX command in SHELXL. Detailed crystallographic data and selected bond lengths and angles are given in Tables S1 and S2 (Supporting Information), respectively.

**Theoretical Calculations.** The ground-state ( $S_0$ ) geometries of 1–3 and their Zn(II) complexes were optimized using the density functional theory (DFT) method with the B3LYP functional<sup>43</sup> and 6-31G(d)<sup>44</sup> basis sets. The structures of the lowest-lying singlet excited state ( $S_1$ ) of 1 and 3 were optimized using the configuration interaction single (CIS) with the 6-31G(d) basis sets. Time-dependent density functional theory (TD-DFT)<sup>45</sup> was used with 6-31G(d) to obtain electronic transition energies which include some accounts of electron correlation. To include the solvation effect of THF, the polarizable continuum model (PCM) was used in the calculations.<sup>46</sup> All calculations were carried out using the GAUSSIAN 09 program.<sup>47</sup>

## ■ ASSOCIATED CONTENT

### ● Supporting Information

Tables, figures, and CIF files giving UV/vis absorption and fluorescence titration results of 1–3 and their Zn(II) complexes and crystallographic data. This material is available free of charge via the Internet at <http://pubs.acs.org>.

## ■ AUTHOR INFORMATION

### Corresponding Author

\*E-mail: [suleechem@ulsan.ac.kr](mailto:suleechem@ulsan.ac.kr) (S.U.L.); [lmh74@ulsan.ac.kr](mailto:lmh74@ulsan.ac.kr) (M.H.L.).

### Notes

The authors declare no competing financial interest.

## ■ ACKNOWLEDGMENTS

This work was supported by the Basic Science Research Program (NRF-2012R1A1A2039773 for M.H.L. and NRF-2013R1A1A2058722 for Y.H.L.) and Priority Research Centers

program (No. 2009-0093818) through the National Research Foundation of Korea (NRF) funded by the Ministry of Education. S.U.L. expresses sincere thanks to the crews of the Center for Computational Materials Science of the Institute for Materials Research, Tohoku University, for their continuous support of the SR1000 supercomputing facilities.

## ■ REFERENCES

- (1) Steed, J. W.; Turner, D. R.; Wallace, K. J. *Core Concepts in Supramolecular Chemistry and Nanochemistry*; Wiley-VCH: Chichester, U.K., 2007. Lehn, J.-M. *Supramolecular Chemistry*; Wiley-VCH: Weinheim, Germany, 1995.
- (2) Kim, S. K.; Sessler, J. L. *Chem. Soc. Rev.* **2010**, *39*, 3784–3809. Gokel, G. W. *Molecular Recognition Receptors for Cationic Guests*. In *Comprehensive Supramolecular Chemistry*; Lehn, J.-M., Atwood, J. L., Davies, J. E. D., MacNicol, D. D., Vögtle, F., Eds.; Pergamon: Oxford, U.K., 1996; Vol. 1.
- (3) Hua, Y.; Flood, A. H. *Chem. Soc. Rev.* **2010**, *39*, 1262–1271. Caltagirone, C.; Gale, P. A. *Chem. Soc. Rev.* **2009**, *38*, 520–563. Kubik, S. *Chem. Soc. Rev.* **2009**, *38*, 585–605. Gale, P. A.; Garcia-Garrido, S. E.; Garric, J. *Chem. Soc. Rev.* **2008**, *37*, 151–190. Gale, P. A.; Quesada, R. *Coord. Chem. Rev.* **2006**, *250*, 3219–3244.
- (4) McConnell, A. J.; Beer, P. D. *Angew. Chem., Int. Ed.* **2012**, *51*, 5052–5061. Kim, S. K.; Lynch, V. M.; Young, N. J.; Hay, B. P.; Lee, C.-H.; Kim, J. S.; Moyer, B. A.; Sessler, J. L. *J. Am. Chem. Soc.* **2012**, *134*, 20837–20843.
- (5) Constable, E. C. *Chem. Soc. Rev.* **2007**, *36*, 246–253. Schubert, U. S.; Hofmeier, H.; Newkome, G. R. *Modern Terpyridine Chemistry*; Wiley-VCH: Weinheim, Germany, 2006.
- (6) Peng, X.; Xu, Y.; Sun, S.; Wu, Y.; Fan, J. *Org. Biomol. Chem.* **2007**, *5*, 226–228.
- (7) Goodall, W.; Williams, J. A. G. *Chem. Commun.* **2001**, 2514–2515.
- (8) Lee, Y. H.; Fuyuhiko, A.; Harrowfield, J. M.; Kim, Y.; Sobolev, A. N.; Hayami, S. *Eur. J. Inorg. Chem.* **2013**, 5862–5870.
- (9) Tan, Y.; Gao, J.; Yu, J.; Wang, Z.; Cui, Y.; Yang, Y.; Qian, G. *Dalton Trans.* **2013**, *42*, 11465–11470. Lee, Y. H.; Kubota, E.; Fuyuhiko, A.; Kawata, S.; Harrowfield, J. M.; Kim, Y.; Hayami, S. *Dalton Trans.* **2012**, *41*, 10825–10831. Bergamini, G.; Boselli, L.; Ceroni, P.; Manca, P.; Sanna, G.; Pilo, M. *Eur. J. Inorg. Chem.* **2011**, *2011*, 4590–4595. Hong, Y.; Chen, S.; Leung, C. W. T.; Lam, J. W. Y.; Liu, J.; Tseng, N.-W.; Kwok, R. T. K.; Yu, Y.; Wang, Z.; Tang, B. Z. *ACS Appl. Mater. Interfaces* **2011**, *3*, 3411–3418. Yang, Z.; Yan, C.; Chen, Y.; Zhu, C.; Zhang, C.; Dong, X.; Yang, W.; Guo, Z.; Lu, Y.; He, W. *Dalton Trans.* **2011**, *40*, 2173–2176. D'Aléo, A.; Cecchetto, E.; De Cola, L.; Williams, R. M. *Sensors* **2009**, *9*, 3604–3626. Hwang, S.-H.; Wang, P.; Moorefield, C. N.; Jung, J.-C.; Kim, J.-Y.; Lee, S.-W.; Newkome, G. R. *Macromol. Rapid Commun.* **2006**, *27*, 1809–1813. Li, Y. Q.; Bricks, J. L.; Resch-Genger, U.; Spieles, M.; Rettig, W. *J. Phys. Chem. A* **2006**, *110*, 10972–10984.
- (10) Zhao, H.; Leamer, L. A.; Gabbai, F. P. *Dalton Trans.* **2013**, *42*, 8164–8178. Wade, C. R.; Broomsgrove, A. E. J.; Aldridge, S.; Gabbai, F. P. *Chem. Rev.* **2010**, *110*, 3958–3984. Jäkle, F. *Chem. Rev.* **2010**, *110*, 3985–4022. Hudson, T. W.; Chiu, C.-W.; Gabbai, F. P. *Acc. Chem. Res.* **2009**, *42*, 388–397. Hudson, Z. M.; Wang, S. *Acc. Chem. Res.* **2009**, *42*, 1584–1596. Cametti, M.; Rissanen, K. *Chem. Commun.* **2009**, 2809–2829.
- (11) Sarkar, S. K.; Thilagar, P. *Chem. Commun.* **2013**, *49*, 8558–8560. Song, K. C.; Lee, K. M.; Nghia, N. V.; Sung, W. Y.; Do, Y.; Lee, M. H. *Organometallics* **2013**, *32*, 817–823. Song, K. C.; Kim, H.; Lee, K. M.; Lee, Y. S.; Do, Y.; Lee, M. H. *Dalton Trans.* **2013**, *42*, 2351–2354. Swamy, P. C. A.; Mukherjee, S.; Thilagar, P. *Chem. Commun.* **2013**, *49*, 993–995. Wade, C. R.; Ke, I.-S.; Gabbai, F. P. *Angew. Chem., Int. Ed.* **2012**, *51*, 478–481. Vadavi, R. S.; Kim, H.; Lee, K. M.; Kim, T.; Lee, J.; Lee, Y. S.; Lee, M. H. *Organometallics* **2012**, *31*, 31–34. Zhao, H.; Gabbai, F. P. *Organometallics* **2012**, *31*, 2327–2335. Song, K. C.; Lee, K. M.; Kim, H.; Lee, Y. S.; Lee, M. H.; Do, Y. *J. Organomet. Chem.* **2012**, *713*, 89–95. Wade, C. R.; Gabbai, F. P. *Organometallics* **2011**,

- 30, 4479–4481. Kim, Y.; Huh, H.-S.; Lee, M. H.; Lenov, I. L.; Zhao, H.; Gabbai, F. P. *Chem. Eur. J.* **2011**, *17*, 2057–2062. Lee, K. M.; Huh, J. O.; Kim, T.; Do, Y.; Lee, M. H. *Dalton Trans.* **2011**, *40*, 11758–11764. Zhao, H.; Gabbai, F. P. *Nat. Chem.* **2010**, *2*, 984–990. Xu, W.-J.; Liu, S.-J.; Zhao, X.-Y.; Sun, S.; Cheng, S.; Ma, T.-C.; Sun, H.-B.; Zhao, Q.; Huang, W. *Chem. Eur. J.* **2010**, *16*, 7125–7133. Matsumoto, T.; Wade, C. R.; Gabbai, F. P. *Organometallics* **2010**, *29*, 5490–5495. Kim, Y.; Zhao, H.; Gabbai, F. P. *Angew. Chem., Int. Ed.* **2009**, *48*, 4957–4960. Wade, C. R.; Gabbai, F. P. *Dalton Trans.* **2009**, 9169–9175. Chiu, C.-W.; Kim, Y.; Gabbai, F. P. *J. Am. Chem. Soc.* **2009**, *131*, 60–61. Kim, Y.; Gabbai, F. P. *J. Am. Chem. Soc.* **2009**, *131*, 3363–3369. Agou, T.; Sekine, M.; Kobayashi, J.; Kawashima, T. *Chem. Eur. J.* **2009**, *15*, 5056–5062. Hudnall, T. W.; Kim, Y.-M.; Bebbington, M. W. P.; Bourissou, D.; Gabbai, F. P. *J. Am. Chem. Soc.* **2008**, *130*, 10890–10891. Hudnall, T. W.; Gabbai, F. P. *Chem. Commun.* **2008**, 4596–4597. Chiu, C.-W.; Gabbai, F. P. *Dalton Trans.* **2008**, 814–817. Lee, M. H.; Gabbai, F. P. *Inorg. Chem.* **2007**, *46*, 8132–8138. Lee, M. H.; Agou, T.; Kobayashi, J.; Kawashima, T.; Gabbai, F. P. *Chem. Commun.* **2007**, 1133–1135. Hudnall, T. W.; Gabbai, F. P. *J. Am. Chem. Soc.* **2007**, *129*, 11978–11986. Chiu, C.-W.; Gabbai, F. P. *J. Am. Chem. Soc.* **2006**, *128*, 14248–14249.
- (12) Ko, S.-B.; Lu, J.-S.; Kang, Y.; Wang, S. *Organometallics* **2013**, *32*, 599–608.
- (13) Song, K. C.; Kim, H.; Lee, K. M.; Lee, Y. S.; Do, Y.; Lee, M. H. *Sens. Actuators B* **2013**, *176*, 850–857.
- (14) Sun, Y.; Hudson, Z. M.; Rao, Y.; Wang, S. *Inorg. Chem.* **2011**, *50*, 3373–3378. Sun, Y.; Wang, S. *Inorg. Chem.* **2009**, *48*, 3755–3767.
- (15) Huh, J. O.; Kim, H.; Lee, K. M.; Lee, Y. S.; Do, Y.; Lee, M. H. *Chem. Commun.* **2010**, *46*, 1138–1140.
- (16) Wade, C. R.; Gabbai, F. P. *Inorg. Chem.* **2010**, *49*, 714–720.
- (17) Sun, Y.; Ross, N.; Zhao, S.-B.; Huszarik, K.; Jia, W.-L.; Wang, R.-Y.; Macartney, D.; Wang, S. *J. Am. Chem. Soc.* **2007**, *129*, 7510–7511.
- (18) Sun, Y.; Wang, S. *Inorg. Chem.* **2010**, *49*, 4394–4404.
- (19) Jia, W.-L.; Bai, D.-R.; McCormick, T.; Liu, Q.-D.; Motala, M.; Wang, R.-Y.; Seward, C.; Tao, Y.; Wang, S. *Chem.—Eur. J.* **2004**, *10*, 994–1006.
- (20) Sakuda, E.; Funahashi, A.; Kitamura, N. *Inorg. Chem.* **2006**, *45*, 10670–10677.
- (21) Hudson, Z. M.; Sun, C.; Harris, K. J.; Lucier, B. E. G.; Schurko, R. W.; Wang, S. *Inorg. Chem.* **2011**, *50*, 3447–3457.
- (22) Hudson, Z. M.; Zhao, S.-B.; Wang, R.-Y.; Wang, S. *Chem. Eur. J.* **2009**, *15*, 6131–6137.
- (23) Hudson, Z. M.; Wang, S. *Organometallics* **2011**, *30*, 4695–4701.
- (24) Rao, Y.-L.; Wang, S. *Inorg. Chem.* **2009**, *48*, 7698–7713.
- (25) Rao, Y.-L.; Schoenmakers, D.; Chang, Y.-L.; Lu, J.-S.; Lu, Z.-H.; Kang, Y.; Wang, S. *Chem. Eur. J.* **2012**, *18*, 11306–11316.
- (26) You, Y.; Park, S. Y. *Adv. Mater.* **2008**, *20*, 3820–3826. Zhao, Q.; Li, F.; Liu, S.; Yu, M.; Liu, Z.; Yi, T.; Huang, C. *Inorg. Chem.* **2008**, *47*, 9256–9264.
- (27) Hudson, Z. M.; Wang, S. *Dalton Trans.* **2011**, *40*, 7805–7816. Hudson, Z. M.; Helander, M. G.; Lu, Z.-H.; Wang, S. *Chem. Commun.* **2011**, *47*, 755–757.
- (28) Kokado, K.; Chujo, Y. *Dalton Trans.* **2011**, *40*, 1919–1923. Schülter, F.; Wild, A.; Winter, A.; Hager, M. D.; Baumgaertel, A.; Friebe, C.; Schubert, U. S. *Macromolecules* **2010**, *43*, 2759–2771. Harriman, A.; Rostron, J. P.; Cesario, M.; Ulrich, G.; Ziessel, R. *J. Phys. Chem. A* **2006**, *110*, 7994–8002.
- (29) Ma, Z.; Cao, Y.; Li, Q.; Guedes da Silva, M. F. C.; Fraústo da Silva, J. J. R.; Pombeiro, A. J. L. *J. Inorg. Biochem.* **2010**, *104*, 704–711.
- (30) Ma, Z.; Liang, B.; Yang, M.; Lu, L. *Acta Crystallogr., Sect. E* **2012**, *68*, m298–m299.
- (31) Zhao, Y.-H.; Pan, H.; Fu, G.-L.; Lin, J.-M.; Zhao, C.-H. *Tetrahedron Lett.* **2011**, *52*, 3832–3835.
- (32) Kawachi, A.; Tani, A.; Shimada, J.; Yamamoto, Y. *J. Am. Chem. Soc.* **2008**, *130*, 4222–4223.
- (33) Sun, H.; Dong, X.; Liu, S.; Zhao, Q.; Mou, X.; Yang, H. Y.; Huang, W. *J. Phys. Chem. C* **2011**, *115*, 19947–19954.
- (34) Henze, O.; Lentz, D.; Schlüter, A. D. *Chem. Eur. J.* **2000**, *6*, 2362–2367.
- (35) Sun, C.; Lu, J.; Wang, S. *Org. Lett.* **2011**, *13*, 1226–1229.
- (36) Potts, K. T.; Konwar, D. *J. Org. Chem.* **1991**, *56*, 4815–4816.
- (37) Brouwer, A. M. *Pure Appl. Chem.* **2011**, *83*, 2213–2228. Melhuish, W. H. *J. Phys. Chem.* **1961**, *65*, 229–235.
- (38) Arvai, A. J.; Nielsen, C. *ADSC Quantum-210 ADX Program*; Area Detector System Corporation, Poway, CA, USA, 1983.
- (39) Otwinowski, Z.; Minor, W., Processing of X-ray Diffraction Data Collected in Oscillation Mode. In *Methods in Enzymology*; Carter, C. W., Sweet, R. M., Eds.; Academic Press: New York, 1997; Vol. 276, pp 307–326.
- (40) Sheldrick, G. M. *SHELXS-97: Program for the Solution of Crystal Structures*; University of Göttingen, Göttingen, Germany, 2008.
- (41) Sheldrick, G. M. *SHELXL-97: Program for the Refinement of Crystal Structures*; University of Göttingen, Göttingen, Germany, 2008.
- (42) Sheldrick, G. M. *Acta Crystallogr., Sect. A* **2008**, *64*, 112–122.
- (43) Stephens, P. J.; Devlin, F. J.; Chabalowski, C. F.; Frisch, M. J. *J. Phys. Chem.* **1994**, *98*, 11623–11627. Lee, C.; Yang, W.; Parr, R. G. *Phys. Rev. B* **1988**, *37*, 785–789.
- (44) Binkley, J. S.; Pople, J. A.; Hehre, W. J. *J. Am. Chem. Soc.* **1980**, *102*, 939–947.
- (45) Runge, E.; Gross, E. K. U. *Phys. Rev. Lett.* **1984**, *52*, 997–1000.
- (46) Mennucci, B.; Tomasi, J.; Cammi, R.; Cheeseman, J. R.; Frisch, M. J.; Devlin, F. J.; Gabriel, S.; Stephens, P. J. *J. Phys. Chem. A* **2002**, *106*, 6102–6113. Cammi, R.; Tomasi, J. *J. Comput. Chem.* **1995**, *16*, 1449–1458. Miertuš, S.; Scrocco, E.; Tomasi, J. *Chem. Phys.* **1981**, *55*, 117–129.
- (47) Frisch, M. J., et al. *Gaussian 09, Revision A.02*; Gaussian, Inc., Wallingford, CT, 2009.